Available online at www.sciencedirect.com
SCIENCE DIRECT®
Journal of Chromatography A, 1030 (2004) 177–186
JOURNAL OF CHROMATOGRAPHY A
www.elsevier.com/locate/chroma

Model column structure for the analysis of the flow and band-broadening characteristics of silica monoliths

Nico Vervoort*, Piotr Gzil, Gino V. Baron, Gert Desmet

Department of Chemical Engineering, Vrije Universiteit Brussel, Pleinlaan 2, 1050 Brussels, Belgium

Abstract

We report on the use of commercial computational fluid dynamics software to study the band broadening in a perfectly ordered three-dimensional model structure, the so-called tetrahedral skeleton column (TSC), selected for its close geometrical resemblance to the specific pore network topology of silica monoliths. Van Deemter plots are presented for the case of a species flow through a non-porous skeleton and for the case of a retained component ($k' = 1$) in a porous skeleton (mesopore porosity $\varepsilon = 0.6$ in both cases). Using the flow domain as the characteristic scaling dimension, the TSC model yields reduced plate heights as small as $h_{min} = 0.8$ and separation impedances as small as $E_{min} = 120$ for a retained component with $k' = 1$. The very small reduced plate heights for the TSC model can without any doubt largely be attributed to the perfect homogeneity of the considered model structure: the B and C terms are similar to those obtained in real silica monoliths with similar external porosity, whereas the A term is significantly (about a factor of 10) smaller. The present study hence suggests that further experimental work to obtain more homogeneous silica networks could yield large gains in reduced plate height and separation impedance. Comparing the three-dimensional TSC model with a 2D array of cylinders, it was found that the use of the domain size as the characteristic dimension in the reduced plate height expression is much more appropriate than the use of the skeleton size, hence validating earlier approaches adopted in the literature.

Keywords: Computational fluid dynamics; Mathematical modelling; Computer simulation; Tetrahedral skeleton column model; Band broadening; Monolithic columns

1. Introduction

In the past few years, the use of monolithic columns has increased in a nearly exponential way [1–4]. Despite of this large interest, the flow properties of the monoliths are still not fully understood, despite of the excellent recent modelling work performed, amongst others, by Liapis et al. [5], Tallarek and co-workers [6,7] and Gritti et al. [8]. One of the remaining problems is that detailed data on the variation of the pressure drop, the eddy-dispersion and the local mass transfer rates with the exact topology of the flow-through pore network are not available.

To exactly predict the band broadening in a porous medium, all microscopic details of the pore structure and the velocity field should be known [9]. Fully solving the flow and species diffusion equations in an exact replicate of a real, heterogeneous silica monolith however lies beyond the presently available computational power. We therefore recently set up a theoretical study [10] to explore the possibility to approximate the entire porous network by a representative unit cell, capable of representing the main pore network characteristics (pore connectivity number, branch connectivity number) but with a sufficient degree of symmetry and isotropy to be used as a unit building block, which, upon translation and/or mirroring, can be used to build an infinitely extending homogeneous pore network. An appealing advantage of this modelling approach is that all the structural properties (porosity, flow-through pore size, specific skeleton surface) of the unit cell can be represented using only two single parameters: the skeleton diameter d_s and the skeleton unit length l_s (Fig. 1). The other geometrical information (branch connectivity, angles between the individual branches) is implicitly known from the definition of the unit cell geometry. By independently varying d_s and l_s, a complete range of possible combinations of bed porosity and skeleton thickness can be covered. With such a small flow domain, detailed data on the flow field and the species transport can easily be calculated using computational fluid dynamics (CFD) software. Combining

* Corresponding author. Tel.: +32-2-629-36-17; fax: +32-2-629-32-48.
E-mail address: nvervoor@vub.ac.be (N. Vervoort).

0021-9673/$ – see front matter © 2004 Elsevier B.V. All rights reserved.
doi:10.1016/j.chroma.2003.12.040

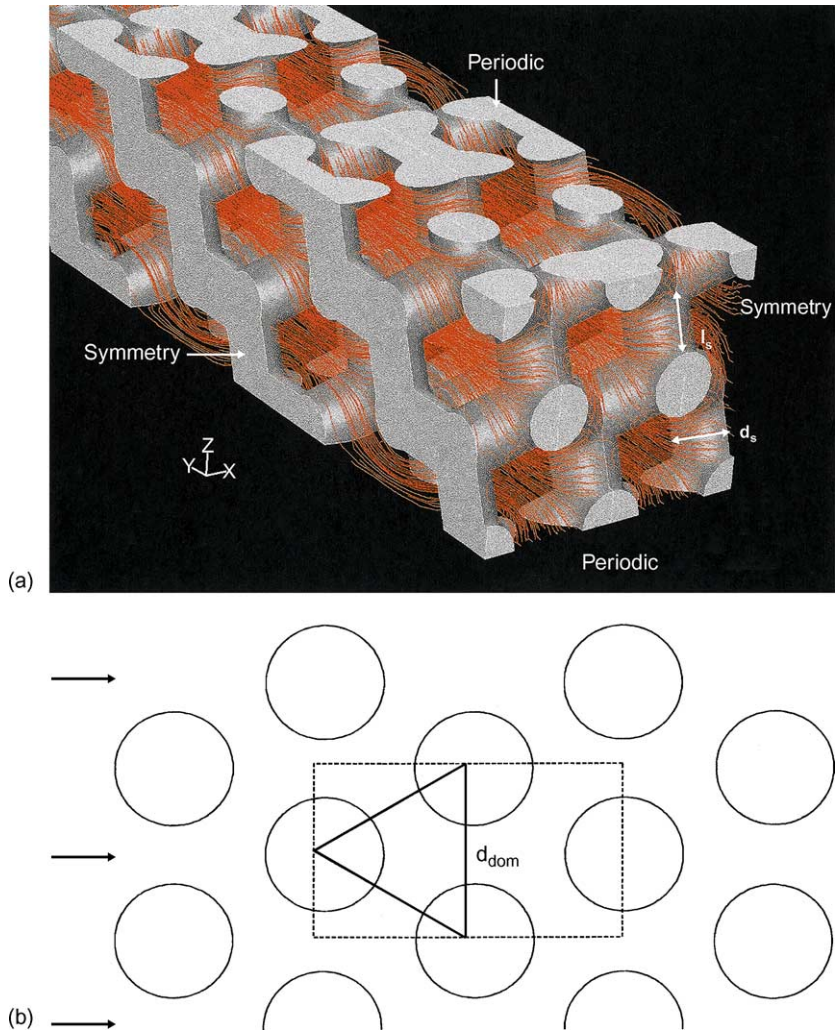

Fig. 1. (a) 3D view of the unit cell of a TSC with $d_s = 1\,\mu m$ and $l_s = 1.35\,\mu m$ ($\varepsilon = 0.603$) and visualisation of the calculated flow field using the particle tracking method of the Fluent® solver. (b) Unit cell of the 2D cylinder array with $\varepsilon = 0.6$, also showing the definition of d_{dom}.

advanced numerical solver and grid generation routines, CFD software packages are namely ideally suited to solve the complete impulse and species conservation balances in complex domains with a high degree of accuracy. Since the dramatic increase in computational power of commercial personal computers and workstations over the last decade, CFD simulations have over the last decade become an important and widely accepted tool in the field of chemical engineering [11], and are now also gradually introduced into the field of chromatography [10,12].

Another advantage of the adopted representative unit cell modelling approach is that it yields insight on how well a perfectly homogeneous pore network would perform as compared to the rather irregular pore network structure of real silica monoliths. The fact that such irregularities (variations on the pore diameter) exist can clearly be seen in published SEM pictures [2,4]. The quantification of this gain will allow to assess the importance of future experimental efforts to obtain more homogeneous monolithic structures.

Based upon a study of scanning electron microscopy (SEM) pictures of true monolithic silica columns, it was decided that the crystal lattice structure of diamond, in which each connection point coordinates four equally long, equidistant branches to its four neighbours, and further referred to as the tetrahedral skeleton column (TSC) structure, displays a branch connectivity (4) and a structural isotropy coming close to the sponge-like geometry of the real monolithic silica beds (Fig. 1). In a recent study [10], we used the simplified geometrical TSC model to establish a direct correlation between the pressure drop and two main structural properties (skeleton thickness and column porosity) of the monolithic skeleton. The correlation shows good agreement (much better than the commonly employed Kozeny–Carman model or equivalent sphere diameter model) with the experimental pressure-drop data available from the literature on silica monoliths, especially when a correction for the flow-through pore size heterogeneity is made.

In the present study, we want to verify whether the TSC model, apart from giving a close fitting pressure-drop

correlation, is also capable of predicting the correct band-broadening characteristics under chromatographic conditions (i.e., for a retained component with $k' = 1$). To evaluate the obtained data, they are compared to the band-broadening data obtained in a non-porous TSC (i.e., for a non-entering and non-retained solute) and to the band broadening in a two-dimensional array of porous cylinders with the same retention factor and porosity. By comparing the peak broadening in the perfectly ordered TSC with the experimental data available in literature (e.g. in [1]), it will be possible to quantify the plate height contribution stemming from the pore network heterogeneity of the current generation of monolithic silica columns.

Before a proper discussion of the band broadening can be made, a suitable characteristic dimension, allowing to bring the band broadening in systems with different pore and skeleton geometry into agreement, is needed. For a packed bed, the selection of this characteristic dimension is obvious, but for the silica monoliths, the problem is much more complex. First, there is the lack of proper geometrical data and the degree of accuracy with which these are obtained (one often has to rely on visual estimates based on SEM pictures of the skeleton), and secondly, there is the problem (at least from a modelling point of view) that the monolith structures have two independent dimensions (one related to the skeleton and one related to the flow-through pores) whose mutual interaction on the flow resistance and the band broadening is up to now not completely understood. An excellent discussion of this problem is given by Tallarek et al. [6]. In the present study, we exploit the availability of exact and complete geometrical data to make an in-depth discussion of the relation between the observable skeleton parameters (skeleton thickness, pore neck size, porosity) and relate them to the flow resistance and band broadening of the monoliths.

2. Considered skeleton geometry and CFD solution methods

The TSC structure used in the flow and species transport simulations was established by appropriately intersecting a number of cylindrical bodies under the right angle, using a commercial CAD program (GAMBIT v.2), acting at the same time as the grid generator for the employed Fluent® 6.1 CFD solver.

To obtain the desired porosity of $\varepsilon = 0.6$, the skeleton diameter was set at 1.0 μm, and the skeleton length l_s (defined as in Fig. 1a) was set at $l_s = 1.35$ μm. With these values, the flow-through pore fraction of the total domain was found to be equal to $\varepsilon = 0.603$ using the volume reporting function of the solver. To vary the porosity, as was needed for the data presented in Fig. 3, the relative magnitude of l_s and d_s was varied as indicated in the caption of Fig. 3. The borders of the unit cell were delimited by intersecting the designed cylindrical skeleton structure with three pairs of orthogonal running cutting planes (in the *x*-, *y*- and *z*-direction). Depending upon whether they act as a symmetry plane or as a translational plane (cf. Fig. 1a), each of these planes is either set as a symmetry wall (slip boundary condition for the calculation of the velocity field and zero normal concentration gradient for the calculation of the species diffusion) or as a periodic wall. With these symmetry and periodic boundary conditions, the flow domain behaves as if it were embedded in an infinitely replicated structure. For the velocity field calculations, a no-slip condition is imposed on the surfaces of the skeleton structure.

For the band-broadening calculations in the non-porous TSC, a zero normal concentration gradient condition was imposed on the skeleton surface. For the simulation of the band broadening under retained solute conditions in the porous TSC, the cylindrical skeleton structure was treated as a continuous porous zone embedded in a continuous fluid zone. The effect of the internal porosity of the skeleton can easily be investigated, as the software package has a built-in function allowing to attribute a given, freely selectable, internal porosity to the porous zone. To approximate the geometry of the silica monoliths, for example, studied in [1] a value of $\varepsilon_{int} = 0.6$ has been adopted in all presented calculations. With the considered external porosity also equal to $\varepsilon = 0.6$, it can easily be calculated that the zone retention factor of the un-retained species are given by:

$$k_0'' = \frac{1-\varepsilon}{\varepsilon}\varepsilon_{int} = 0.4 \quad (1)$$

To mimic the effect of adsorptive retention, a user defined function (UDF) was written to subject the species present in the porous zone to an adsorptive reaction with equilibrium constant *K*. The details of the UDF are described elsewhere [13]. In the present study, all data presented for the porous TSC and the porous 2D array of cylinders (Fig. 1b) were obtained by putting $K = 3.5$. Combining the latter value with the $\varepsilon = 0.6$ value taken for the external porosity, it can easily be calculated that the zone retention factor k'' [14] for all considered porous column cases was equal to $k'' = 1.8$:

$$k'' = (1+K)\frac{1-\varepsilon}{\varepsilon}\varepsilon_{int} = 1.8 \quad (2)$$

Considering then that the phase retention factor k' can be calculated as [14]:

$$k' = \frac{k'' - k_0''}{1 + k_0''} \quad (3)$$

it can easily be calculated that all presented porous column calculations relate to a retained component with phase retention factor $k' = 1$.

To mimic the effect of the slow intra-skeleton diffusivity, a second UDF (details also given in [13]) was used to attribute the species entering the stationary phase zone a diffusion coefficient (D_s) different (i.e., smaller) from that in the fluid zone (D_m). In the present study, D_s was put at 5×10^{-10} m^2/s, i.e., two times smaller than the diffusivity in the through pore region. The latter assumption corresponds roughly to

the data on the D_m to D_s ratio in silica monoliths recently given by Tallarek et al. [6].

Water, with a density of 1000 kg/m3 and a viscosity of 1.003×10^{-3} kg/(ms), was chosen as the working fluid. The corresponding Reynolds numbers (based upon the skeleton diameter as the characteristic length) were typically of the order 10^{-5} to 10^{-6}, such that it can safely be concluded that the flow conditions were always strictly laminar. The pore volume space was discretized with an unstructured tetrahedral grid. All calculations were carried out on Dell personal computers with Intel Xeon 2 GHz processor, and equipped with 2 Gb RAM.

By monitoring the radially averaged species concentration at nine successive detection planes regularly spaced along the axial coordinate of the flow domain as a function of time, mean peak migration times and peak variances were calculated using a numerical integration scheme based on the trapezoid's rule and implemented in a Microsoft Excell® worksheet, using:

$$t_{R,i} = \frac{\int_0^{+\infty} C_i t \, \mathrm{d}t}{\int_0^{+\infty} C_i \, \mathrm{d}t} \tag{4}$$

$$\sigma_{t,i}^2 = \frac{\int_0^{+\infty} C_i t^2 \, \mathrm{d}t}{\int_0^{+\infty} C_i \, \mathrm{d}t} - t_R^2 \tag{5}$$

Combining Eqs. (4) and (5), theoretical plate height values were calculated according to:

$$H = \frac{\sigma_{t,j}^2 - \sigma_{t,i}^2}{(t_{R,j} - t_{R,i})^2} L_{ij} \tag{6}$$

From Eq. (4), phase and zone retention factors (k' and k'') can be calculated as:

$$t_{R,i} = \frac{L_i}{u_0}(1 + k') = \frac{L_i}{u_m}(1 + k'') \tag{7}$$

The validity of the obtained results was always checked by comparing the mean migration time of the simulated peak with the expected value based on $t_R = L/u_m(1 + k'')$. This always corresponded to within less than 0.5%. It was also always verified whether the σ_t^2 values obtained at different distances $\times$ along the flow domain varied in a linearly proportional way with the distance $\times$ in the flow domain, as should be the case according to the theory of chromatography [15].

To compare the three-dimensional TSC with a 2D system, we also conducted a series of retained solute simulations in a 2D domain system composed of a series connection of the unit cell depicted in Fig. 1b. For these series of simulations, all parameters were taken equal to those used for the porous TSC. The diameter of the cylinders was, for example, set equal to the skeleton size of the TSC, i.e., $d = 1\,\mu$m. To consider a system with a maximal isotropy, the cylinders were arranged in a so-called equilateral staggered conformation, i.e., the centre points of neighbouring pillars are situated on the corners of an equilateral triangle.

Prior to its use in the currently considered, relatively complex geometry, the adopted combination of the CFD solver with the self-written user defined functions has been validated by comparing the simulated band broadening between two parallel infinite planes, each coated with a thick stationary phase layer ($d_s = 0.5\,$d), with the analytical solution established by Golay and Aris [13]. The difference was always smaller than 0.3% for all considered mobile phase velocities.

In the simulations, it is also assumed that the transport through the porous skeleton zone occurs by pure molecular diffusion (with effective diffusivity D_s), i.e., it is assumed that there is no convective transport through the skeleton. This assumption can easily be justified by considering that the ratio of through pore to meso-pore sizes in a typical monolith is of the order of 100, as was shown by Tallarek et al. [6].

3. Results and discussion

3.1. Flow-through pore diameter determination and pressure drop

Fig. 1a shows how the streamlines continuously merge and split as they flow through the skeleton. The streamlines also indicate how the flow can be divided in tubular bundles with a given diameter. Finding the value of this characteristic flow-through pore diameter is a tedious problem, and has thus far only been approached by rather crude methods, such as the direct visual inspection of SEM pictures. Using the advanced data processing methods of the Fluent® solver, it is however quite easy to determine the pore diameter at each desired cross-sectional plane (Fig. 2). In the present study, we focused on the determination of the minimal pore cross-section (pore neck), as this is what one would intuitively measure when assessing the flow-through pore width from a SEM picture. Fig. 2 shows how the minimal pore section can be determined in the 3D TSC structure. Once the plane cutting through the pore neck is identified, the cross-sectional area of the pore neck is easily obtained using the surface area report function of the Fluent® solver. From this value (A_{por}), it is straightforward to define the quantity $d_{por,1}$ as the diameter of the circle having the same cross-sectional area:

$$d_{por,1} = \sqrt{\frac{4}{\pi} A_{por}} \tag{8}$$

Fig. 3 gives the $d_{por,1}$ values obtained according to the method presented in Fig. 2 for a wide range of different porosities. The data are reduced on the basis of the skeleton diameter, because the definition of the TSC is such that all geometrical parameter ratio's are fixed by the selection of the porosity, a characteristic which also seems to hold in real silica monoliths, given the fact that columns with the same porosity but with a different skeleton thickness approximately yield the same d_{por}/d_s ratio, as can, for

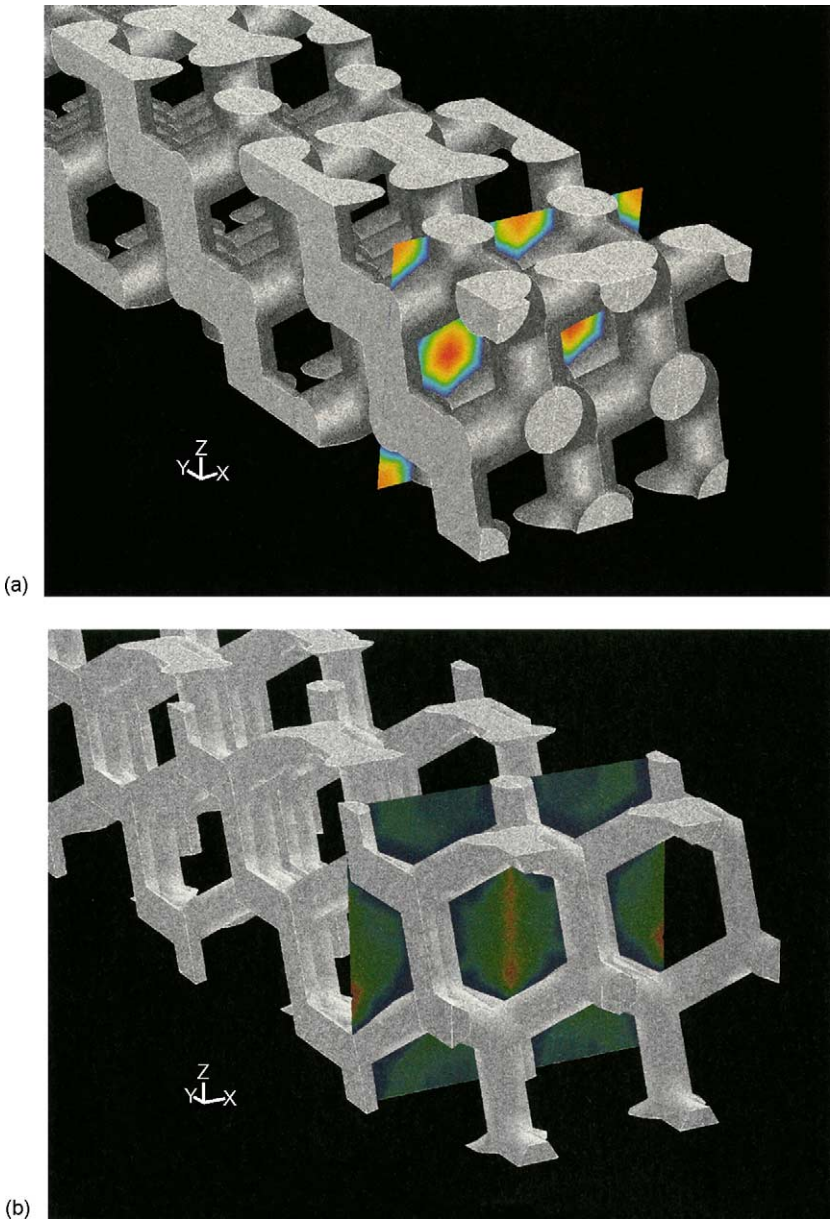

Fig. 2. Determination of the characteristic through pore size d_{por} for a TSC with $\varepsilon = 0.603$ (a) and $\varepsilon = 0.864$ (b).

example, be noted from the data in [16]. This feature enlarges the general applicability of the data in Fig. 2. For the sake of comparison, we also considered an alternative pore diameter estimation method. This was based on the expression for the pressure drop in a cylindrical tube with given diameter:

$$d_{por,2} = \sqrt{\frac{32 u_m \eta L}{\Delta P}} \tag{9}$$

In Eq. (9), L represent the length along the tortuous path of the column. Given that the tortuosity in the bed only varies between $\tau = 1.18$ ($\varepsilon = 0.4$) and $\tau = 1.02$ ($\varepsilon = 0.95$) [10], the difference with the linear bed length is however very small. u_m represents the interstitial velocity. This generally is an unknown quantity, but with the definition of the bed permeability K_v:

$$K_v = \frac{u_m \eta L}{\Delta P} \tag{10}$$

Eq. (9) can easily be written as:

$$d_{por,2} = \sqrt{32 K_v} \tag{11}$$

Eq. (11) constitutes a very simple expression, and as is shown, fits nicely to the $d_{por,1}$ values determined from the minimal through pore area. This implies that it should be possible to determine d_{por} from the measured K_v, and inversely, predict K_v on the basis of the minimal pore size determined from a visual SEM picture inspection. As can be noted, the $d_{por,1}$ and $d_{por,2}$ values both also agree well with the experimental data given in [1,4].

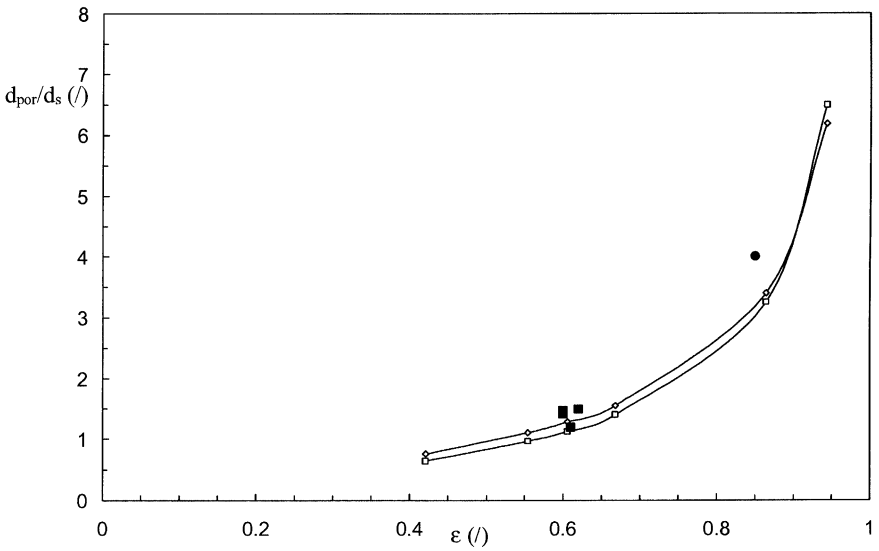

Fig. 3. Plot of $d_{por,1}/d_s$ (cf. Eq. (8)) and $d_{por,2}/d_s$ (cf. Eq. (9)) vs. the bed porosity for the TSC model (open symbols) and comparison with the experimental values given in [1] (square solid symbols) and [4] (round solid symbol). The different considered porosities were obtained by keeping the skeleton diameter at $d_s = 1\,\mu m$, and by varying l_s as follows: $l_s = 1.05\,\mu m$ ($\varepsilon = 0.421$); $l_s = 1.25\,\mu m$ ($\varepsilon = 0.554$); $l_s = 1.50\,\mu m$ ($\varepsilon = 0.668$); $l_s = 2.50\,\mu m$ ($\varepsilon = 0.864$); $l_s = 4.00\,\mu m$ ($\varepsilon = 0.943$).

To bring the above considerations on the relation between the pore size and the pressure drop further, more detailed data are needed. In this respect, approaches such as the one adopted in [17], wherein laser scanning confocal microscopy techniques are combined with a marching cubes algorithm to obtain exact 3D numerical replicates of the internal structure of monolith columns, seem to be very promising.

3.2. Band-broadening calculations

Fig. 4 shows the evolution of a virtual inject plug of tracer species through a porous TSC. The band broadening is clearly observable. It can also be noted how some of the species are longer withheld in the skeleton and lags behind the main peak. Simulations as the one shown in Fig. 4 have been repeated for a wide range of inlet velocities.

Fig. 5 compares the plate height values obtained on the basis of Eqs. (4)–(6) for the porous TSC, the non-porous TSC and the porous 2D system. As was expected, the porous TSC and 2D columns ($k'' = 1.8$) yields much larger plate heights than the non-porous equivalents ($k'' = 0$). More interesting is the relatively large difference between the 2D and the TSC column when compared for the same k''. Since both systems have the same external and internal porosity, the same retention factor, have stationary phase zones with the same cylindrical shape and with the same diameter ($d = 1\,\mu m$), the relatively large difference between the van Deemter curves reflects the fact that the skeleton diameter is not an appropriate reduction basis, as was already noted by, amongst others, Minakuchi et al. [1] and Knox [18]. Whereas they preferred the total domain size over the skeleton diameter to obtain a better agreement between the silica monolith and the packed bed of spheres, i.e., to let the reduced plate heights for the monoliths come closer to that of the packed bed (for which it is a quasi universally valid rule that $h_{min} = 2$), the inadequacy of the skeleton diameter as a useful reduction factor is now again confirmed from a new point of view, i.e., by comparing a 2D with a 3D system with the same skeleton diameter.

To further investigate the use of the domain size as a better suited reduction basis, Fig. 6 shows the data of Fig. 5 obtained after a transformation based on:

$$h = \frac{H}{d_{dom}} \quad \text{and} \quad \nu_0 = \frac{u_0 d_{dom}}{D_m} \tag{12}$$

One of the main differences between the 2D and the 3D system is that, although both systems have the same porosity and the same stationary zone shape and diameter, their domain size is significantly different. With the data from Fig. 3, and defining d_{dom} as the sum of d_s and d_{por}, as commonly adopted in the field [1,3,4], a value of $d_{dom} = 2.28\,\mu m$ is obtained. For the 2D column, d_{dom} is defined in Fig. 1b. For the $d = 1\,\mu m$ case, it can easily be verified that $d_{dom} = 1.5\,\mu m$, i.e., indeed significantly smaller than for the 3D TSC.

As can be noted from Fig. 6, there is now a much better agreement between the 2D column and the TSC. The agreement is however not perfect, showing that the domain size can also not be considered as the ultimate characteristic dimension allowing to bring the plate height values of systems with a different geometry into perfect agreement. Obviously, more research is needed to gain more insight in the problem.

Also shown in Fig. 6 is the experimental reduced plate height correlation established by Minakuchi et al. [1] for a series of monolith columns with a porosity around 0.6, and also obtained using the domain size as the reduction basis. As can be noted, the difference between the porous TSC and the experimental data is very large.

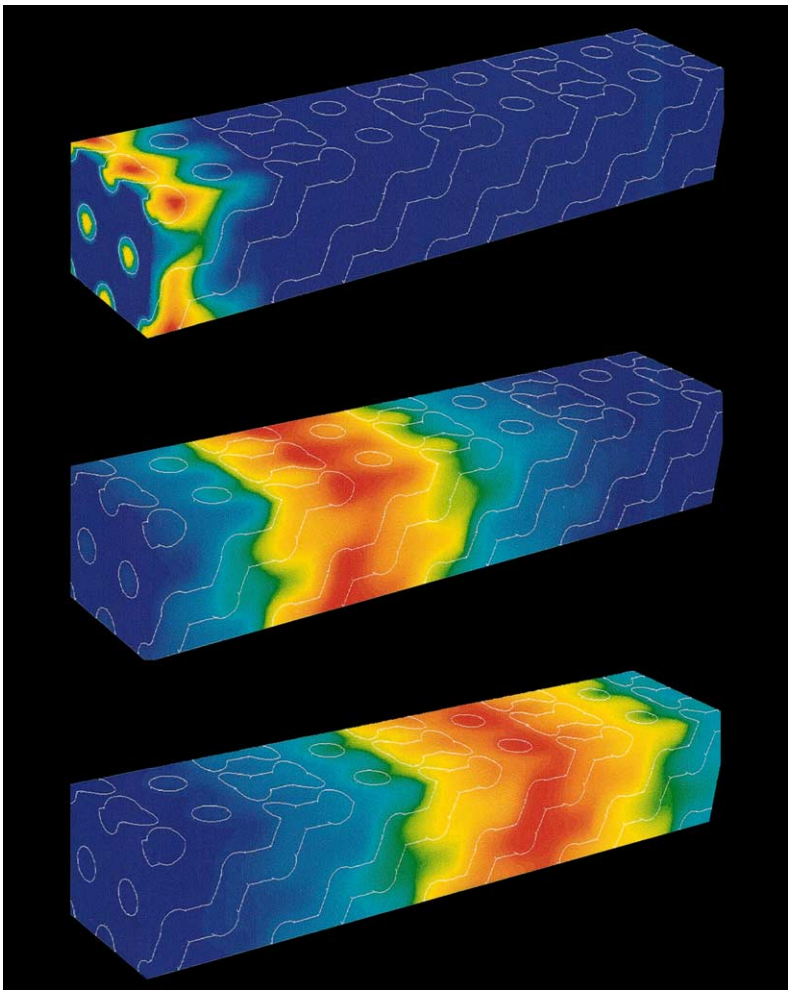

Fig. 4. Simulated passage of a virtual inject plug of tracer species through a four unit cell long TSC with $\varepsilon = 0.6$ ($u_m = 5.5$ mm/s, $k' = 1$, $d_s = 1\,\mu$m and $l_s = 1.35\,\mu$m).

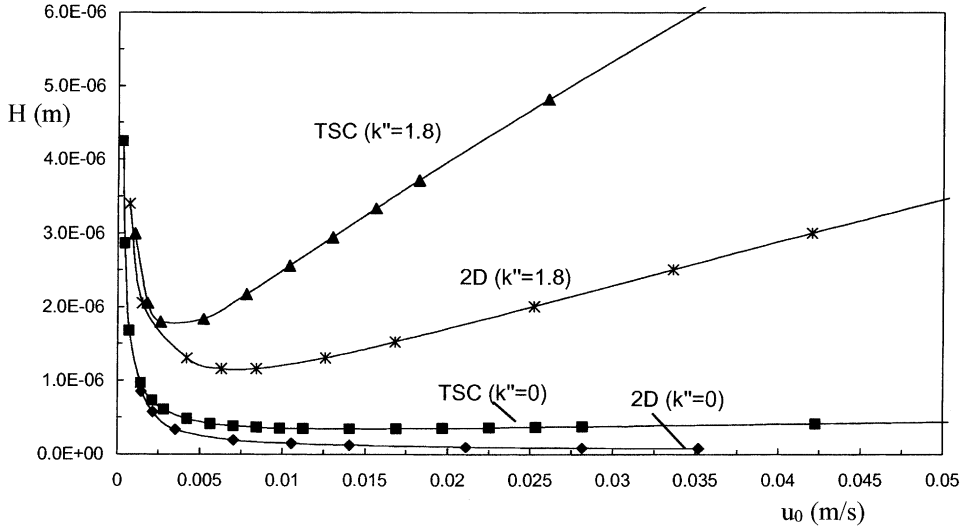

Fig. 5. Plot of H vs. u_0 for the 3D porous and non-porous TSC and for the 2D porous and non-porous cylinder array (column porosity $\varepsilon = 0.6$ in all cases, other simulation conditions given in the text).

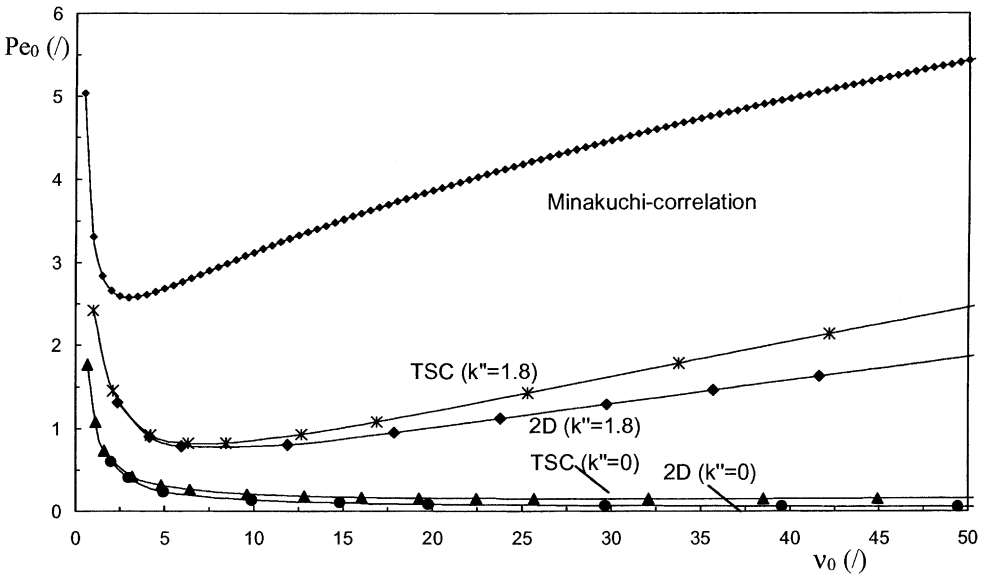

Fig. 6. Data of Fig. 5 replotted as h vs. ν_0, using $d_{dom} = 2.28\,\mu m$ to reduce the TSC data and $d_{dom} = 1.5\,\mu m$ to reduce the 2D column data. The data are also compared with the experimental correlation established by Minakuchi et al. [1]: $h = 1.3\,\nu_0^{1/3} + 2/\nu_0 + 0.012\,\nu_0$.

To gain more insight in this difference, the reduced plate height curve for the porous TSC column shown in Fig. 6 has been fitted with Knox's well-established reduced plate height expression:

$$h = A\nu^{1/3} + \frac{B}{\nu} + C\nu \tag{13}$$

Using the solver function of Microsoft Excell to conduct a simultaneous three parameter fit, the following values for the Knox parameters were obtained: $A = 0.13$, $B = 2.31$ and $C = 0.02$. Whereas the B and C values lie surprisingly close to the Minakuchi parameters (resp. $B = 2$ and $C = 0.012$, see the caption of Fig. 6), the decrease of the A term (from $A = 1.3$ for the true monoliths to $A = 0.13$ for the TSC) is really dramatic. For the perfectly ordered 2D pillar array comparable values were obtained ($A = 0.15$, $B = 1.68$ and $C = 0.07$). Since the A term represents the contribution to the band-broadening stemming from the flow-through pore heterogeneity [4,18], the large discrepancy between the real monolithic columns and the TSC model clearly stems from the perfect homogeneity of the pore structure in the TSC model. Reversing this argument, this result, in fact, shows the large gains which could be obtained if much more homogeneous porous separation media would be available. We believe it is the first time this gain is quantified. The presently observed strong dependency of h on the pore heterogeneity also substantiates the argumentation made in [1], wherein the increasing deviation (towards larger h) from the

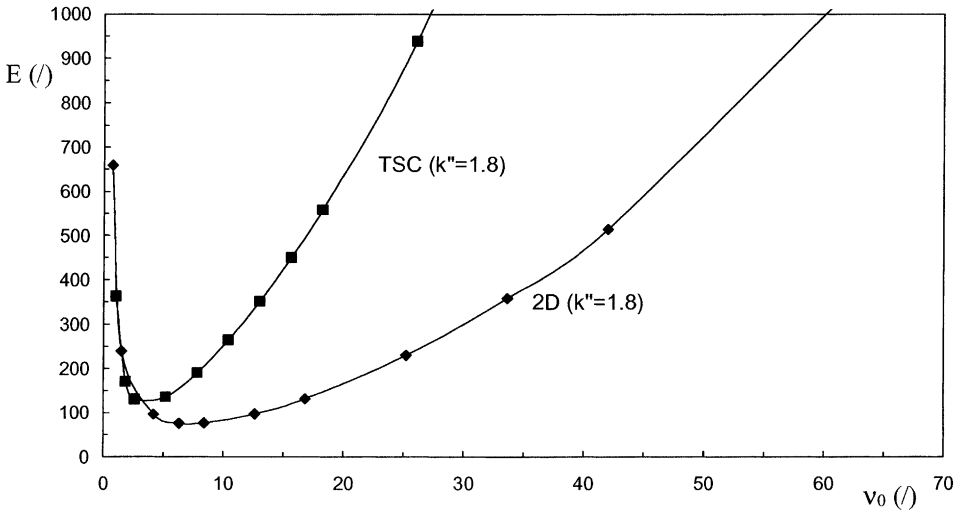

Fig. 7. Plot of E vs. u_0 for the porous TSC model ($k' = 1$ case, same simulation conditions as in Figs. 5 and 6).

Minakuchi correlation for the columns with the smallest domain size was blamed on the increased heterogeneity of the flow-through pores.

Fig. 7 gives the separation impedances calculated on the basis of the H values shown in Fig. 5 and on the bed permeabilities ($K_{v0} = 1.31 \times 10^{-14}$ for the TSC and $K_{v0} = 2.47 \times 10^{-14}$ for the 2D column) calculated from our velocity calculations. Again, the perfectly ordered TSC, yielding a value of $E_{min} \cong 120$, performs better than the real, disordered silica monoliths with the same $\varepsilon = 0.6$ monoliths studied in [1], for which values between 300 and 700 were obtained. The influence of the column model structure geometry will be investigated in the near future, but so far only small differences have been found, and the large difference with the real, disordered monoliths remains. More detailed results on this will be the topic of a future publication.

4. Conclusion

A theoretical proof for the often raised assumption that the plate height in silica monoliths is to a large extent determined by the pore heterogeneity is obtained. Improved monolith performances should hence not immediately be improved by making smaller through pores, but rather by making them more uniform. The expected gain is dramatic. Using the domain size as the basis of reduction, minimal plate heights below $h_{min} = 1$, should be obtainable, whereas the best possible silica monoliths yield values around $h_{min} = 2.5$. The optimal velocity also shifts significantly: from $v_0 = 2$ for the real monoliths to $v_0 = 7$ for the perfectly homogeneous TSC. Whether or not it will ever be possible to make silica monoliths with a sufficiently homogeneous pore network to achieve the predicted gain is very uncertain, but, having now quantified the expected gain, we believe the present study should encourage future research efforts aiming at the generation of more homogeneously structured porous separation media.

5. Nomenclature

A_{por}	cross-sectional pore area (m^2)
d	cylinder diameter (m)
d_{dom}	domain size (m, $d_{dom} = d_s + d_{por}$ for the TSC; for the 2D column, d_{dom} is defined as shown in Fig. 1b)
d_l	TSC skeleton length (m)
d_{por}	flow-through pore diameter determined as shown in Fig. 2 (m)
d_s	TSC skeleton diameter (m)
h	reduced theoretical plate height ($h = H/d_{ref}$)
H	height equivalent of a theoretical plate (m)
k'	phase retention factor
k''	zone retention factor
K	adsorption equilibrium constant
K_v	bed permeability based on u_m (m^2)
K_{v0}	bed permeability based on u_0 (m^2)
l_{sm}	mean skeleton length (m)
L	column length (m)
L_{ij}	distance between two different detection planes i and j (m)
Δp	pressure drop (Pa/m)
$t_{R,i}$; $t_{R,j}$	mean passage time at detection planes i and j (s)
u_0	mean velocity of permeating, but non-retained solute (m/s)
u_m	mean velocity of moving fluid = velocity of non-permeating solute (m/s)
u_{sf}	superficial velocity (m/s)

Greek letters

ε	extra-skeleton porosity
ε_{int}	intra-skeleton porosity
ϕ	flow resistance
η	viscosity ($kg\,m^{-1}\,s^{-1}$)
v_0	reduced fluid velocity, based on u_0 ($u_0 d_p/D_{mol}$)
σ_t^2	peak variance (s^2)
τ	tortuosity

Acknowledgements

The authors greatly acknowledge a research grant (FWO KNO 81/00) of the Fund for Scientific Research-Flanders (Belgium). P.G. is supported through a specialization grant from the Instituut voor Wetenschap en Technologie (IWT) of the Flanders Region (grant No. SB/11419).

References

[1] H. Minakuchi, K. Nakanishi, N. Soga, N. Ishizuka, N. Tanaka, J. Chromatogr. A 797 (1998) 121.
[2] N. Tanaka, H. Kobayashi, K. Nakanishi, H. Minakuchi, N. Ishizuka, Anal. Chem. (2001) 420.
[3] N. Tanaka, H. Nagayama, H. Kobayashi, T. Ikegami, K. Hosoya, N. Ishizuka, H. Minakuchi, K. Nakanishi, K. Cabrera, P. Lubda, J. High Resolut. Chromatogr. 23 (2000) 111.
[4] N. Tanaka, H. Kobayashi, N. Ishizuka, H. Minakuchi, K. Nakanishi, K. Hosoya, T. Ikegami, J. Chromatogr. A 965 (2002) 35.
[5] A.I. Liapis, J.J. Meyers, O.K. Crosser, J. Chromatogr. A 865 (1999) 13.
[6] U. Tallarek, F.C. Leinweber, A. Seidel-Morgenstern, Chem. Eng. Technol. 25 (2002) 1177.
[7] F.C. Leinweber, D. Lubda, K. Cabrera, U. Tallarek, Anal. Chem. 74 (2002) 2470.
[8] F. Gritti, W. Piatkowski, G. Guiochon, J. Chromatogr. A 983 (2003) 51.
[9] A.J. Sederman, M.L. Johns, P. Alexander, L.F. Gladden, Chem. Eng. Sci. 53 (1998) 2117.
[10] N. Vervoort, P. Gzil, G.V. Baron, G. Desmet, Anal. Chem. 75 (2003) 843.
[11] K.R. Westerterp, R.J. Wijngaarden, N.B.G. Nijhuis, Chem. Eng. Technol. 19 (1996) 291.

[12] Y.X. Wu, C.B. Chin, Chromatographia 56 (2002) 679.
[13] P. Gzil, N. Vervoort, G.V. Baron, G. Desmet, Anal. Chem. 75 (2003) 6244.
[14] J. Knox, H.P. Scott, J. Chromatogr. 282 (1983) 297.
[15] J.C. Giddings, Dynamics of Chromatography, Part I, Marcel Dekker, New York, 1965.
[16] N. Ishizuka, H. Minakuchi, K. Nakanishi, N. Soga, H. Nagayama, K. Hosoya, N. Tanaka, Anal. Chem. 72 (2000) 1275.
[17] H. Jinnai, K. Nakanishi, Y. Nishikawa, J. Yamanaka, T. Hashimoto, Langmuir 17 (2001) 619.
[18] J.H. Knox, J. Chromatogr. A 960 (2002) 7.